Liquid Crystals
Publication details, including instructions for authors and subscription information:
http://www.informaworld.com/smpp/title~content=t713926090

Influence of K_{24} on the structure of nematic liquid crystal droplets

S. Žumer[a]; S. Kralj[b]
[a] Physics Department, University of Ljubljana, Ljubljana, Slovenia [b] Faculty of Education, University of Maribor, Maribor, Slovenia

To cite this Article Žumer, S. and Kralj, S.(1992) 'Influence of K_{24} on the structure of nematic liquid crystal droplets', Liquid Crystals, 12: 4, 613 — 624
To link to this Article: DOI: 10.1080/02678299208029097
URL: http://dx.doi.org/10.1080/02678299208029097

LIQUID CRYSTALS, 1992, VOL. 12, NO. 4, 613–624

Influence of K_{24} on the structure of nematic liquid crystal droplets

by S. ŽUMER* and S. KRALJ†
Physics Department, University of Ljubljana, Jadranska 19,
61000 Ljubljana, Slovenia
† Faculty of Education, University of Maribor, Koroška 160,
62000 Maribor, Slovenia

(*Received 18 February 1992; accepted 17 April 1992*)

A phenomenological free energy is used to describe the stable ordering of nematic liquid crystals confined to supramicron spherical cavities. In particular the effects of the saddle splay elastic constant, K_{24}, on the equilibrium structures and phase diagram of droplets with homeotropic surface anchoring are discussed. Some structures are illustrated by the corresponding simulated polarization microscope textures. Possibilities for an experimental determination of the saddle-splay elastic constant and surface anchoring strength by studying the radial–axial structural transition in such droplets are analysed. It is shown that the K_{24} term in the elastic free energy stabilizes a deformed droplet structure even in the limit of the zero anchoring strength.

1. Introduction

Most of the studies of the surface effect on nematic liquid crystals have dealt with director anchoring, more precisely with the angular dependent part of the interfacial coupling [1–3]. These phenomena are particularly important for the operation of the twist and supertwist nematic cells [4]. Usually the effect of the surface part of the elastic free energy is neglected [5]. This approach is justified in the strong anchoring limit where a fixed anchoring angle can be assumed. When liquid crystals are confined to micron size spaces this limit is not usually applicable. This is the case in the recently discovered polymer dispersed liquid crystals (PDLC) [6] which are used in shutters and displays based on field controlled light scattering [7]. Usually, droplets of a nearly uniform size are formed during the phase separation caused by a polymerization process of liquid crystal–prepolymer mixtures. The average droplet radius varies from the submicron region up to a hundred microns depending on the conditions during the formation process. The nematic structure within a droplet is the result of the interplay between elastic, surface and external field interactions. In submicron droplets the spatial dependence of the order parameter [9–11] and the order parameter dependence of the interfacial coupling [2, 9, 10] are particularly important; therefore the Landau–de Gennes description [12] is usually used. Here we limit our attention to micron and supramicron droplets where a description based on the Frank elastic free energy [13] including surface terms can be used [14]. The effect of the Frank elastic constants K_{11}, K_{22} and K_{33} on the stability of nematic structures is relatively well understood while

* Author for correspondence.

0267–8292/92 $3·00 1992 Taylor & Francis Ltd.

the influence of the twist–bend (K_{13}) and saddle–splay (K_{24}) surface elastic constants [15–19] is much less understood.

In our recent paper [14] we have demonstrated that in the limit of weak anchoring the constant K_{24} influences the director field within a nematic droplet and the stability of structures themselves. Strigazzi was the first to propose a way to measure [16] the K_{24} constant. The difficulty in separating the effects of the surface elastic constant K_{24} and surface anchoring strength was first solved by a ^{2}H NMR study of nematic liquid crystals confined to cylindrical cavities [20, 21] with surfaces enforcing weak normal anchoring. Crawford *et al.* [21] have estimated K_{24} by fitting experimental deuterium spectra with the corresponding line-shapes calculated for the escaped radial structures with point defects.

In contrast to the elastic constants K_{11}, K_{22}, K_{33} and K_{24}, the constant K_{13} is associated with the free energy term which also includes second derivatives of the nematic director field. Its effect has yet to be completely analysed [15–18]. For the appropriate treatment of this elastic constant the bulk elastic terms in the expression for the nematic free energy should be extended up to second order in the second derivatives of the director field $\mathbf{n}$. There is no experimental evidence on the value of K_{13}. A theoretical study in a planar liquid crystal cell indicates limits of possible K_{13} values, namely $K_{13} < K_{33}/2$ and $K_{13} < K_{11}/2$ [17]. In addition Barbero *et al.* [18] have demonstrated that the K_{13} term can stabilize deformed structures although the anchoring strength at the liquid crystal interface is negligible. Therefore the term corresponding to K_{13} will be omitted in the following discussion.

The aim of this paper is to demonstrate how K_{24} and the anchoring strength could be determined by studying the stability diagrams of structures in a spherical nematic droplet embedded in a material which enforces weak homeotropic [22] surface anchoring. In our numerical study we limit our attention to relatively large droplets (supramicron sizes) so that the nematic structures are well characterized by director fields alone [10, 11].

In § 2 we define all contributions to the free energy which are important for our phenomenological treatment of confined nematics. In § 3 the radius–field–temperature phase diagram in supramicron size droplets is briefly discussed. In § 4 the possibility for the determination of the K_{24} elastic constant and surface anchoring strength via the observation of structural transitions in such systems is analysed.

2. Free energy

The minimization of the phenomenological free energy is usually used to determine the stable structure of a chosen system at constant temperature and volume. It is convenient to divide the free energy density into homogeneous f_0, elastic f_e, interfacial f_s and field f_f parts. In our study limited to supramicron droplets a constant order parameter approximation can be used so that f_0 is just a temperature dependent parameter. The inhomogeneous part of the nematic free energy density f_e is thus reduced to the Frank elastic free energy density [5, 12, 23]

$$f_e(\mathbf{r}) = \tfrac{1}{2}\{K_{11}(\nabla\cdot\mathbf{n})^2 + K_{22}(\mathbf{n}\cdot\nabla\times\mathbf{n})^2 + K_{33}(\mathbf{n}\times\nabla\times\mathbf{n})^2 - K_{24}\nabla\cdot(\mathbf{n}(\nabla\cdot\mathbf{n}) + \mathbf{n}\times\nabla\times\mathbf{n})\}, \quad (1)$$

described with four elastic constants. Close to the nematic–isotropic transition T_{NI} these constants are proportional to the square of the order parameter S and so diminish

on approaching T_{NI} [23]. The interaction of the liquid crystal with the surrounding medium is described by a simple contact interaction

$$f_s(\mathbf{r}) = (1-(\mathbf{n}\cdot\mathbf{e}_r)^2)\frac{W_0}{2}\delta(\mathbf{r}-\mathbf{R}), \tag{2}$$

characterized by $\mathbf{e}_r$, the preferred anchoring direction on the droplet surface and the anchoring strength W_0 [1, 2, 24]. The temperature dependence of W_0 can be introduced formally by an expansion in terms of the order parameter S [2]. The vector $\mathbf{R}$ in equation (2) defines points on the droplet surface. The interaction with an external magnetic field $\mathbf{B}$ is described by [23]

$$f_f = -\frac{\mu_0}{2}\Delta\chi(\mathbf{B}\cdot\mathbf{n})^2, \tag{3}$$

where $\Delta\chi$ is the difference between the principal values of the susceptibility tensor corresponding to the directions parallel and perpendicular to $\mathbf{n}$. The material constant $\Delta\chi$ is proportional to the order parameter S [23]. It should be stressed that the effect of an electric field is in general more complicated: in a much larger susceptibility, in comparison to the magnetic case, usually the electric field varies substantially over the droplet. Therefore, a complete solution of the electric field case can be obtained by solving the corresponding Maxwell equations simultaneously with the minimization of the free energy [25]. Further we do not take into account the flexoelectric effect [5] because the flexoelectric free energy (in zero external electric field) is, for typical values of flexoelectric constants, negligible compared to the elastic free energy.

The minimization of the total free energy

$$F = \int (f_0 + f_e + f_s + f_f) d^3\mathbf{r},$$

is achieved by solving the Euler–Lagrange differential equations. We limit our discussion to cases without twist deformations, so the nematic director can be expressed as

$$\mathbf{n} = -\sin\theta\mathbf{e}_\vartheta + \cos\theta\mathbf{e}_r,$$

where $\mathbf{e}_r$ and $\mathbf{e}_\vartheta$ are unit vectors of the spherical coordinate system and θ is the angle between $\mathbf{e}_r$ and $\mathbf{n}$. With this ansatz the Euler–Lagrange equations are reduced to the bulk and surface differential equation for the scalar field $\theta(r, \vartheta)$ where the latter equation introduces boundary conditions imposed by the surface interaction (see equation (2)). The equations are solved by the over relaxation method [26]. Here we concentrate on the effects of the elastic constant K_{24} while all details will be published separately [14].

3. Stable structures and phase diagrams

Within our imposed limitations three simple structures can occur: (i) the radial structure with a central point defect and a mostly radial director field (see structure (*a*) in figure 1); (ii) the axial structure where the director field is predominantly axial in the central region while close to the surface it bends but not enough to satisfy completely the preferred normal anchoring condition at the surface (see structure (*b*) in figure 1); (iii) the axial structure with a line defect (equatorial disclination line) where the director field in the central region is similar to the axial case (ii) but the bend deformation close

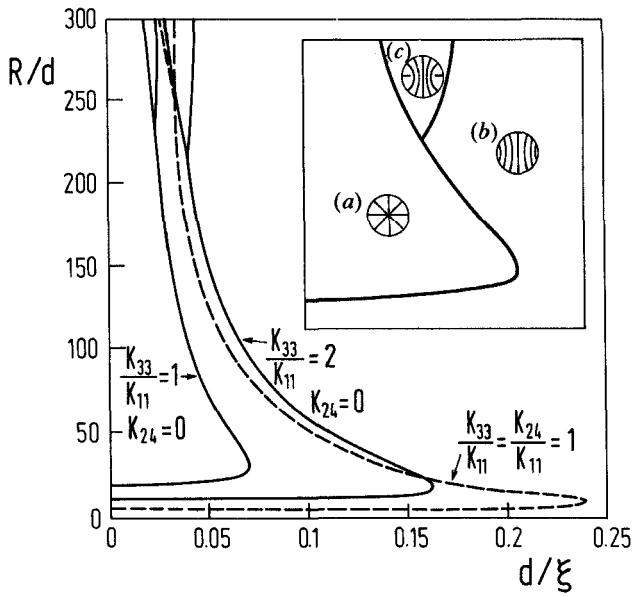

Figure 1. Phase diagram of a nematic droplet with homeotropic anchoring. Coexistence lines for three sets of elastic constants are shown. In the insert schematic representations of stability regions of (*a*) a radial, (*b*) an axial, and (*c*) an axial structure with a line defect are shown.

to the surface is more pronounced so that the director field is nearly everywhere normal to the surface (see structure (*c*) in figure 1).

For a chosen droplet radius a structure may become stable or reversed either by a variation of the external field or indirectly by a temperature induced variation of the material constants. In order to compare the effects of the external field and elastic forces we use the correlation length $\xi = \sqrt{[K_{11}/(\mu_0 \Delta\chi)]}/B$ and to compare the effects of anchoring and elastic forces the extrapolation length $d = K_{11}/W_0$ is used [5].

The stability regions of the structures mentioned can be presented in a universal two dimensional phase diagram (see figure 1) where the ratio $R/d = W_0 R/K_{11}$ on one coordinate axis measures the relative anchoring strength and the ratio $d/\xi = B\sqrt{(K_{11}\mu_0\Delta\chi)}/W_0$ on the other coordinate axis measures the relative field strength. Two neighbouring stability regions are separated by a first order phase transition curve which is described by the dependence of the transition ratio $(d/\xi)_t$ ($\propto B_t$-transition field) on the ratio (R/d). For each set of elastic constants this curve starts at the zero field radial–axial coexistence point $\{0, (R/d)_0\}$ and reaches the inversion point $\{(d/\xi)_i, (R/d)_i\}$ corresponding to the maximum radial–axial transition field $B_{t\,max}$. At the triple point where all three phases coexist, the radial–axial transition line splits into two first order transition lines. Comparison of the phase diagrams for different choices of elastic constants (see figure 1) shows that they all have the same general features but they are substantially scaled along both coordinate axes. It is evident that the contribution of the K_{33} term to the free energy is the largest in the axial structure, smaller in the axial structure with the line defect and the smallest in the radial structure. Similar effects could be observed for the K_{24} contribution. More details of K_{24} dependence will be given in the next section.

We now briefly review the important features of the structures. Radial and axial structures at the zero field coexistence point $\{0,(R/d)_0\}$ are presented in figure 2. In figure 3 the radial and axial structures at the triple point are shown. The radial structure is stable for strong anchoring and weak fields. In zero field the central defect is surrounded by a completely radial director field (see figure 2 (*a*)) which with increasing external field progressively deforms and partially aligns along the direction of the external field but the defect stays at the droplet centre (see figure 3 (*a*)). The axial structure is stable in the weak anchoring regime or for any anchoring strength if the field is stronger than B_t (see figures 2 (*b*) and 3 (*c*)). The degree of the internal director alignment depends on the field and anchoring strength. The axial structure with a defect line in the equatorial plane (see figure 3 (*b*)) is stable only in the strong anchoring limit (above the triple point) in a very narrow region between radial and axial stability regions (see figure 1).

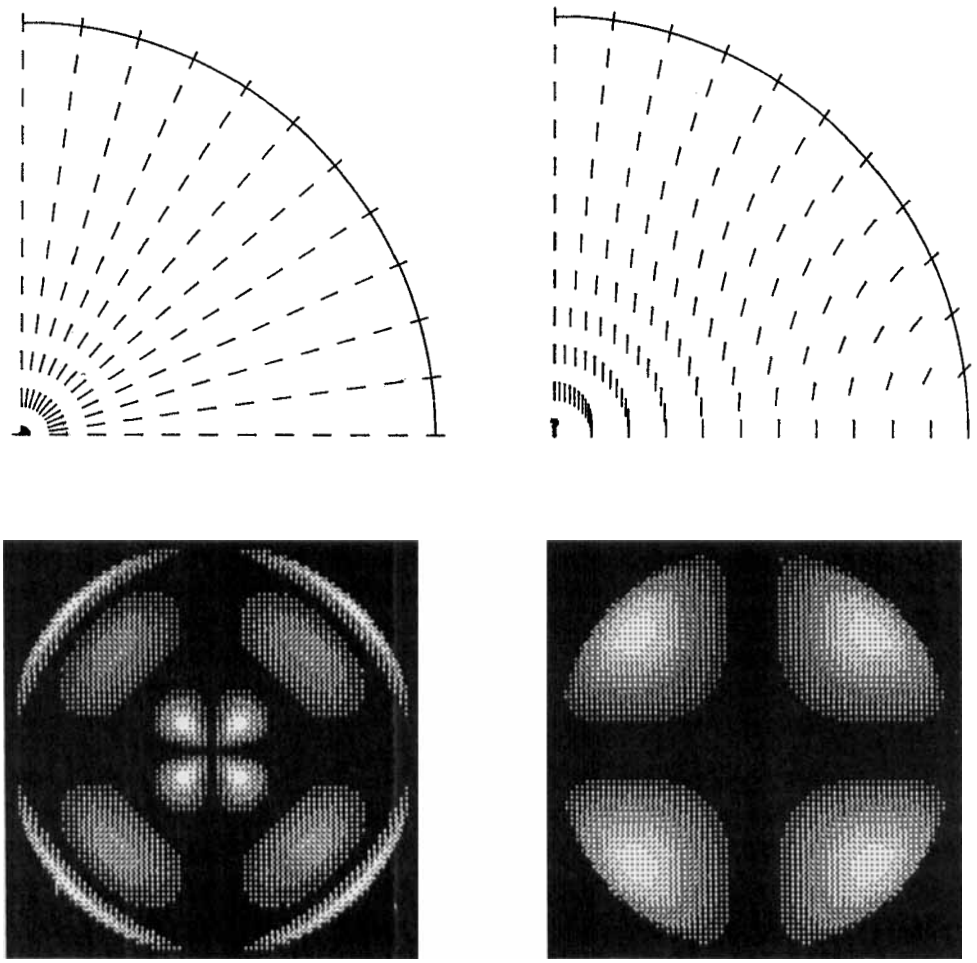

(*a*) (*b*)

Figure 2. Radial (*a*) and axial (*b*) director field and texture of a spherical nematic liquid crystal droplet with homeotropic anchoring at the zero field axial–radial coexistence point. Simulations correspond to $R/\lambda=6$, $K_{11}=K_{33}=K_{24}$, $(R/d)_0=5$.

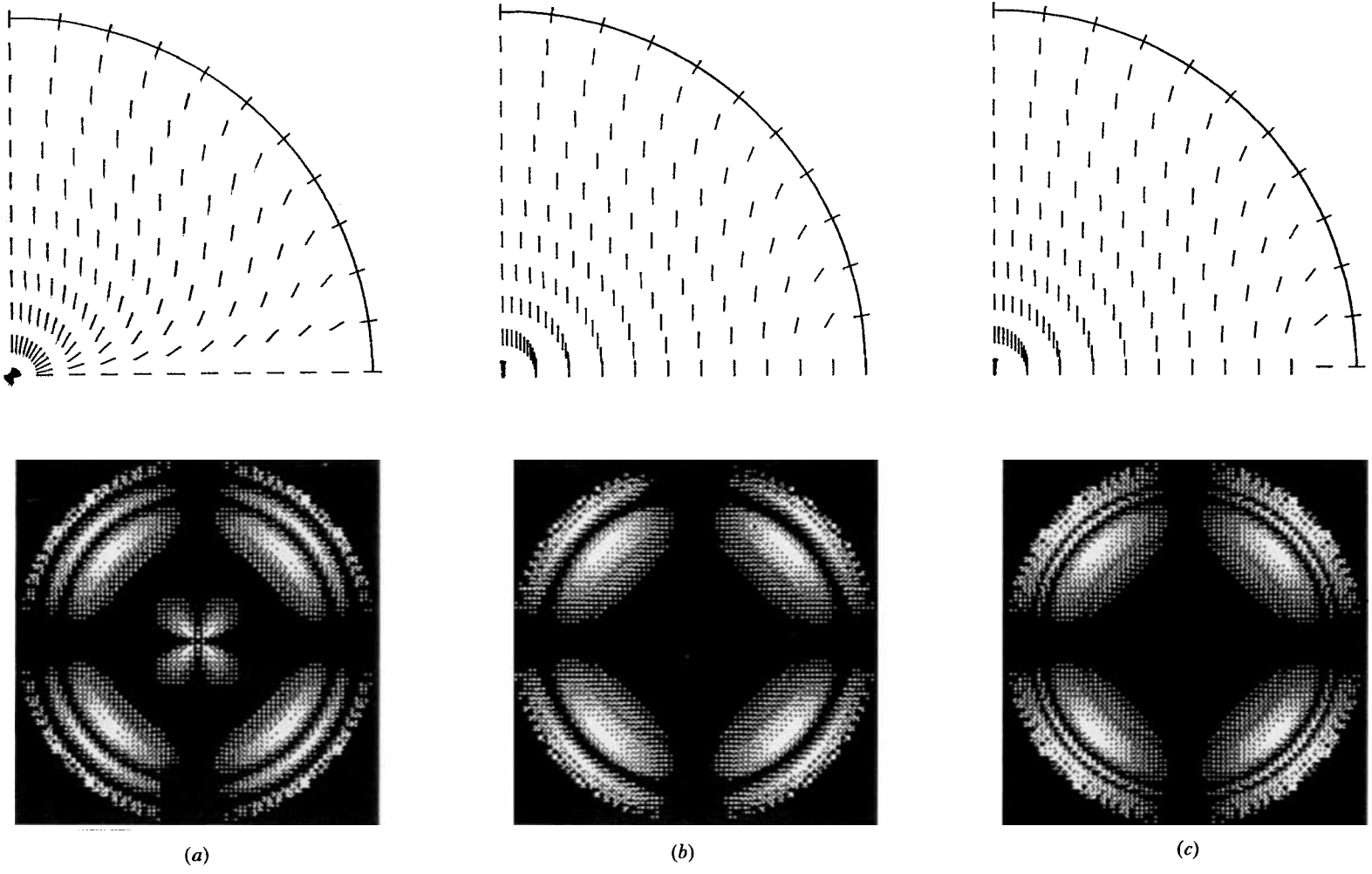

(a) (b) (c)

Figure 3. Director fields of: (*a*) a radial, (*b*) an axial with a defect, (*c*) an axial without a defect and the corresponding textures at the triple point ($(R/d)_i = 250$ and $(d/\xi)_i = 0{\cdot}04$). $K_{11} = K_{33} = K_{24}$ and $R/\lambda = 28$ were used.

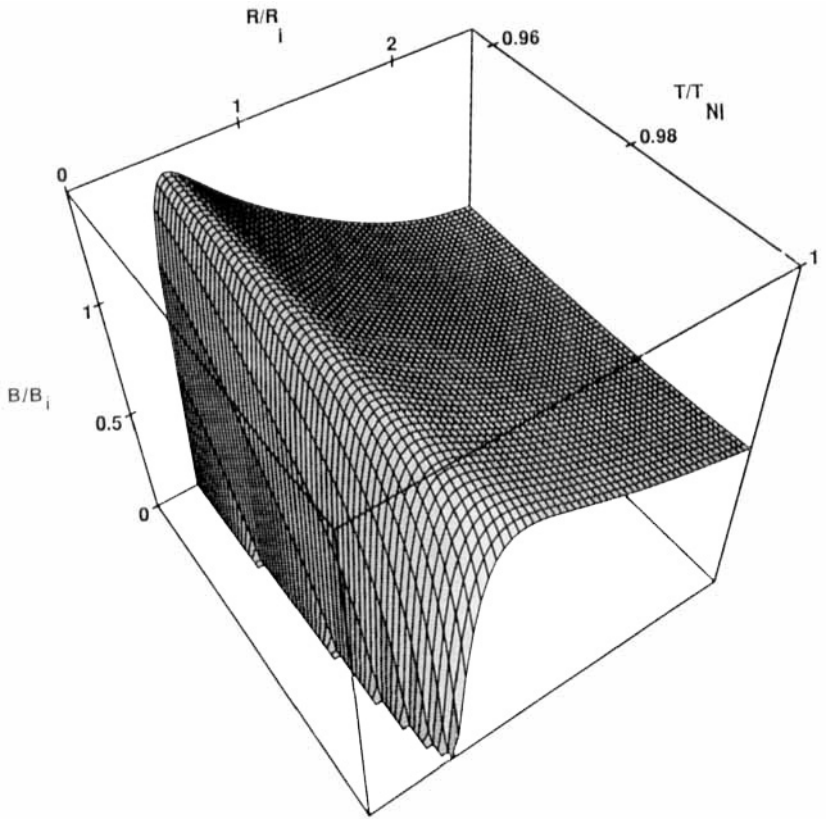

Figure 4. Three dimensional B–R–T phase diagram for a spherical nematic droplet with $K_{11}=K_{33}=K_{24}=K$. Only the weak anchoring region is shown. In the calculations we have assumed $K \propto S(T)^2$, $\Delta\chi \propto S(T)$, $W_0 \propto S(T)$; the temperature dependence of the order parameter $S(T)$ for 4-*n*-pentyl-4′-cyanobiphenyl was used.

In figures 2 and 3 the calculated director fields are accompanied by the corresponding simulated polarization microscope textures. These simulations were obtained with a simple method developed by Crawford *et al.* [27] for the case where differences in indexes of refraction are so small that only phase shifts between the ordinary and extraordinary rays are important while bending and reflection of the rays can be neglected. In our simulations we take 1·7 for the principal index of refraction along the director and 1·5 for the perpendicular direction. In the case of the axial structure only simulations where light is directed along their symmetry axis are treated. Therefore both our textures (axial and radial) have a dark cross as a sign of the cylindrical symmetry but the distributions of the interference fringes are very different reflecting the different spatial dependence of the director field encountered by the passing light.

The universal phase diagram (see figure 1) is useful for the presentation of field-induced transitions because a change in the field strength corresponds to the displacement along the d/ξ axis. The diagram is much less appropriate for the visualization of the temperature-induced transitions because of the temperature dependences of the characteristic lengths d and ξ. Therefore we take into account the

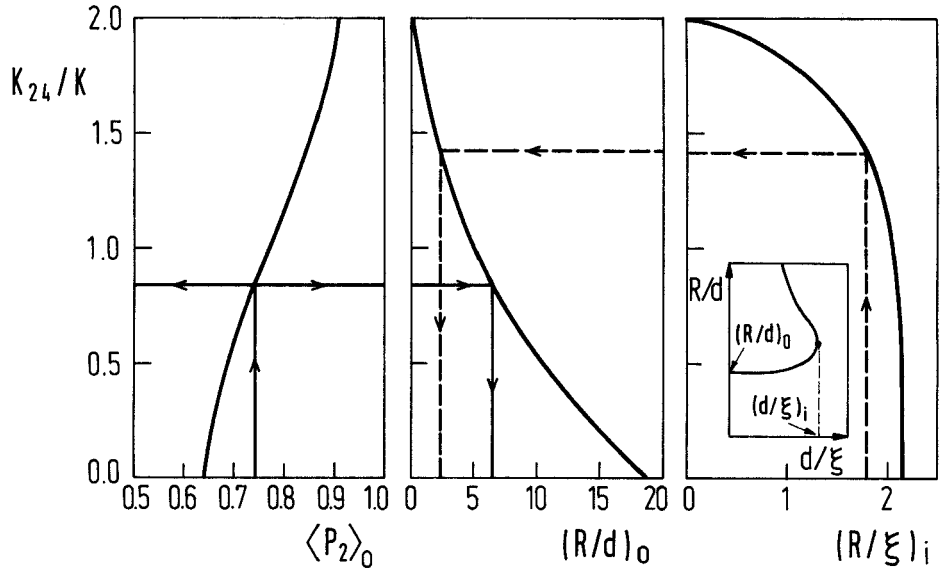

Figure 5. K_{24}/K_{11} dependencies of (*a*) the droplet order parameter $\langle P_2(\cos\theta)\rangle$; (*b*) the ratio $(R/d)_0$ at the zero field coexistence point; (*c*) the ratio $(d/\xi)_i$ at the inversion transition point. In the calculations we have set $K_{11}=K_{33}=K$.

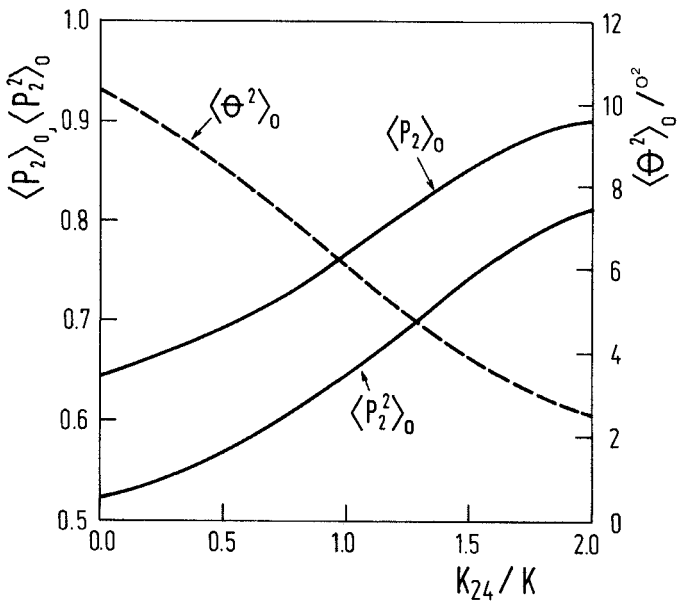

Figure 6. Zero field axial–radial transition point. The dependence of $\langle P_2(\cos(\theta))\rangle_0$, $\langle P_2(\cos(\theta))^2\rangle_0$ and $\langle\theta^2\rangle_0$, measuring the average degree of director alignment, on K_{24}/K for the case $K_{11}=K_{33}=K$.

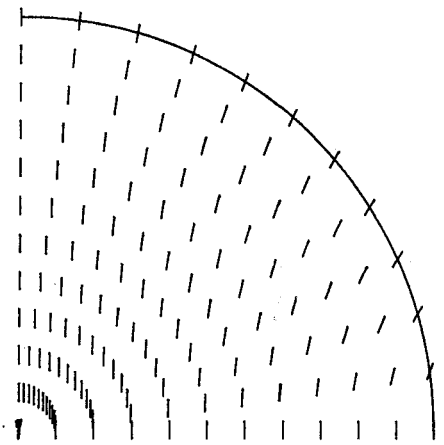

Figure 7. Axial director field at the point $R/d=0$, $d/\xi=0$ which is still stable in the limit $K_{24}/K_{11}\rightarrow 2$.

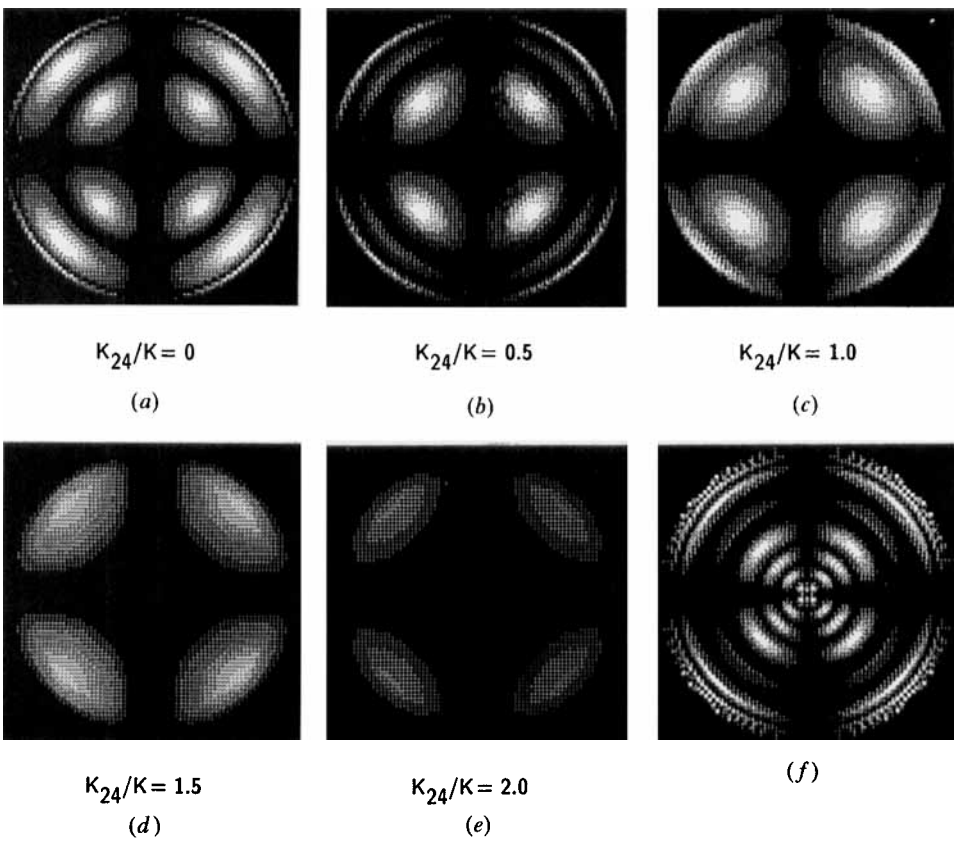

Figure 8. Axial textures (*a*), (*b*), (*c*), (*d*), (*e*) and radial texture (*f*) at zero field axial–radial coexistence point for different K_{24}/K ratios. The approximation of equal Frank elastic constants and the ratio $R/\lambda=20$ were used. The radial texture does not depend on the K_{24}/K ratio but only on the ratio R/λ.

temperature dependence of the elastic constants, $\Delta\chi$, W_0 and create a three dimensional phase diagram where the axes are the quantities field, radius and temperature which can be varied directly (see figure 4). The variables are given in units of the values B_i, R_i, and T_{NI} corresponding to the inversion point $\{(d/\xi)_i, (R/d)_i\}$ at the nematic–isotropic transition temperature T_{NI}.

In the following we discuss how the value of the K_{24} elastic constant can be extracted from the stability diagrams.

4. Determination of K_{24}

For the sake of simplicity we limit our discussion here to the case of equal Frank elastic constants ($K_{11}=K_{33}=K$). To obtain a quantitive measure of changes in a chosen droplet structure we introduce the droplet order parameter defined as

$$\langle P_2\rangle = \langle (3\cos^2\theta - 1)/2\rangle,$$

where θ is the angle between the symmetry axis of the axial structure and the local director field and $\langle\ldots\rangle$ stands for the average over the droplet. Since the zero field coexistence point for all K_{24} values lies in the weak anchoring regime, the axial structure apparently changes with the saddle-splay elastic constant. In figure 5 (*a*) the droplet order parameter $\langle P_2\rangle_0$ of the axial structure at the zero field transition point $\{0,(R/d)_0\}$ is shown as a function of the ratio K_{24}/K. The corresponding dependence of $(R/d)_0$ on K_{24} is plotted in figure 5 (*b*). The dependence of the scaled field $(R/\xi)_i$ corresponding to the inversion point on K_{24} is shown in figure 5 (*c*). We see that by increasing the ratio K_{24}/K, the weak anchoring stability range of the axial structure shrinks and at $K_{24}/K=2$ disappears (see figure 5 (*b*)). Simultaneously the position of the inversion point in the universal phase diagram (see figure 5 (*c*)) shifts towards the zero value of $(R/d)_i$ and the infinite value of $(d/\xi)_i$. Therefore, the existence of the axial structure of a spherical nematic droplet with homeotropic boundary conditions in zero external field is enough to conclude $K_{24}/K_{11}<2$.

It is important to emphasize that $\langle P_2\rangle_0<1$ at $K_{24}/K=2$ indicates that the K_{24} term in a spherical nematic droplet would stabilize a deformed structure also in the case of zero surface interaction strength. This means that the K_{24} term in the free energy effectively plays a similar role to the surface anchoring term. This effect is even more evident in figure 6 where $\langle P_2\rangle_0$, $\langle P_2^2\rangle_0$ and $\langle\theta^2\rangle_0$ dependencies on the K_{24} value are shown and in figure 7 where the calculated stable axial structure at $(R/d)_0=0$ is presented for the case $K_{24}/K=2$. The deformed structure at $(R/d)_0=0$ in figure 8 (*e*) is clearly visible. Similar effects induced by a K_{13} term in the free energy were predicted by Barbero *et al.* [18] for a nematic phase confined to a planar cell.

4.1. *Zero field coexistence point*

The K_{24} value could be extracted from the known $\langle P_2\rangle_0$ value for the axial structure at this point. $\langle P_2\rangle_0$ could be measured, for example, by using the NMR line shape study. With this value for the droplet order parameter the value of the K_{24} can be deduced directly from the numerically calculated functional dependence $\langle P_2\rangle_0=\langle P_2\rangle_0(K_{24}/K_{11})$ for a particular nematic liquid crystal. This procedure is presented schematically by solid lines with arrows in figure 5 (*a*). Further, the anchoring strength can be obtained by introducing the value of K_{24} into the numerically evaluated function $(R/d)_0=(R/d)_0(K_{24}/K_{11})$. In figure 5 (*b*) our single elastic constant case is illustrated.

In larger droplets ($R \gg$ wavelength λ) instead of measuring $\langle P_2 \rangle_0$ the direct optical polarization microscope observations can be used to determine K_{24} at the zero field axial–radial coexistence point. The sequence of calculated textures of the axial structure at this transition point (see figure 8) corresponding to five different K_{24}/K ratios shows a pronounced K_{24} dependence. With increasing K_{24} the intensity and number of interference rings diminishes reflecting increased ordering along the axis of cylindrical symmetry.

4.2. *Inversion point*

Experimental determination of the transition field strength B_i corresponding to the inversion point value $(R/\xi)_i$ leads, together with the known material constants K_{11} and K_{33}, to the determination of K_{24}/K_{11} using a theoretically predicted curve $(R/\xi)_i = (R/\xi)_i(K_{24}/K_{11})$ for a particular choice of K_{33}/K_{11}. This curve and the schematic way of determination is shown in figure 5 (*c*) (see dashed-line with arrows) for $K_{11} = K_{33} = K$. The resulting value of K_{24}/K_{11} could again be used to extract the anchoring strength from the calculated dependence of the zero field coexistence point $(R/d)_0$ dependence on the K_{24}/K_{11} (see dashed line with arrows in figure 5 (*b*)).

5. Conclusions

In this paper we have analysed the influence of the K_{24} constant on the stability of structures of a spherical nematic droplet with a homeotropic boundary condition. Until recently in most studies of encapsulated liquid crystals the contribution corresponding to this elastic constant has been neglected. Our results indicate that such approximations are not justified. Preliminary experiments [20] show that the value of K_{24} is comparable to the values of other Frank elastic constants. Here we have demonstrated how the K_{24} saddle-splay elastic constant can be determined from the zero field and inversion radial–axial transition. Two methods have been proposed: first based on the observation of the structure changes at the zero field axial–radial coexistence point and the other on the determination of the transition field at the inversion point. In combination with theoretical prediction K_{24} and W_0 can be obtained. For small droplets NMR can be used and for large droplets polarization microscopy. In addition we have shown that the presence of the K_{24} term also in the case of the negligible surface interaction strength stabilizes strongly deformed structures in nematic droplets.

The first phase diagram study of a nematic droplet was performed by Erdmann *et al.* [22]. Unfortunately no reliable data on the internal field were available thus preventing the use of the inversion transition point data to obtain K_{24} and W_0. The proved existence of the zero field axial structure is enough to conclude that in the materials studied by Erdmann *et al.* [22] $K_{24} < 2K_{11}$ in accordance with the deuterium NMR data obtained by Allender *et al.* [20]. To overcome the problem of the internal field we must either make a theoretical estimate of the electric field in the nematic droplet or carry out experiments with a magnetic instead of an electric field.

The estimated error of the first experimental determination of K_{24} by ^{2}H NMR [20] is quite large (up to 80 per cent). We believe that our method based on the direct observation of the structure changes in a particular droplet can give more accurate results than the indirect NMR observation of the changes in a large number of not completely identical cavities.

This work was partially supported by NSF grant Solid State Chemistry DMR88-17647 and Science and Technology Centre ALCOM DMR89-20147.

References

[1] COGNARD, J., 1982, *Molec. Crystals liq. Crystals*, **1**, 1.
[2] GOOSSENS, W. J. A., 1985, *Molec. Crystals liq. Crystals*, **124**, 305.
[3] JEROME, B., 1991, *Rep. Prog. Phys.*, **54**, 391.
[4] SCHEFFER, T. J., and NEHRING, J., 1984, *Appl. Phys. Lett.*, **45**, 1021.
[5] DE GENNES, P., 1974, *The Physics of Liquid Crystals* (Clarendon), Chap. 3.
[6] DOANE, J. W., VAZ, N. A., WU, B. G., and ŽUMER, S., 1986, *Appl. Phys. Lett.*, **48**, 269.
[7] DOANE, J. W., 1991, *Math. Res. Soc. Bull.*, **16**, 22.
[8] DOANE, J. W., GOLEMME, A., WEST, J. L., WHITEHEAD, J. B., and WU, B. G., 1988, *Molec. Crystals liq. Crystals*, **165**, 51.
[9] SHENG, P., 1982, *Phys. Rev.* A, **26**, 1610.
[10] KRALJ, S., ŽUMER, S., and ALLENDER, D. W., 1991, *Phys. Rev.* A, **34**, 2943.
[11] VILFAN, I., VILFAN, M., and ŽUMER, S., 1990, *Phys. Rev.* A, **40**, 4724.
[12] PRIESTLEY, E. B., WOJTOWITZ, P. J., and SHENG, P., 1974, *Introduction to Liquid Crystals* (Plenum Press), Chap. 6.
[13] FRANK, F. C., 1958, *Discuss. Faraday Soc.*, **25**, 19.
[14] KRALJ, S., and ŽUMER, S., 1992, *Phys. Rev.* A, **45**, 2461.
[15] NEHRING, J., and SAUPE, A., 1971, *J. chem. Phys.*, **54**, 337; 1972, *J. chem. Phys.*, **56**, 5527.
[16] STRIGAZZI, A., 1987, *Molec. Crystals liq. Crystals*, **152**, 435.
[17] BARBERO, G., and STRIGAZZI, A., 1984, *J. Phys. Lett., Paris*, **45**, 857.
[18] BARBERO, G., MADHUSUDANA, N. V., and OLDANO, C., 1989, *J. Phys., Paris*, **50**, 2263.
[19] SCHMID, V. H., 1990, *Phys. Rev. Lett.*, **64**, 535.
[20] ALLENDER, D. W., CRAWFORD, G. P., and DOANE, J. W., 1991, *Phys. Rev. Lett.*, **67**, 1442.
[21] CRAWFORD, G. P., ALLENDER, D. W., DOANE, J. W., VILFAN, M., and VILFAN, I., 1991, *Phys. Rev.* A, **44**, 2570.
[22] ERDMANN, J. H., ŽUMER, S., and DOANE, J. W., 1990, *Phys. Rev. Lett.*, **64**, 1907.
[23] VERTOGEN, G., and DE JEU, W. H., 1988, *Thermotropic Liquid Crystals* (Springer Verlag), Chap. 3.
[24] RAPINI, A., and PAPOULAR, M., 1969, *J. Phys., Paris*, **30**, 54.
[25] HAAS, G., WOHLER, H., FRITSCH, M. W., and MLYNSKI, D. A., 1991, *Molec. Crystals liq. Crystals*, **198**, 15.
[26] PRESS, W. H., FLANNERY, B. P., TEUKOLSKY, S. A., and VETTERLING, W. T., 1986, *Numerical Recipes* (Cambridge University Press), Chap. 17.
[27] OMDRIS-CRAWFORD, R. O., BOYKO, E. P., WAGNER, B. G., ERDMANN, J. H., ŽUMER, S., and DOANE, J. W., 1991, *J. appl. Phys.*, **69**, 6380.